Translational Research in Anatomy 40 (2025) 100425

Contents lists available at ScienceDirect

Translational Research in Anatomy

journal homepage: www.elsevier.com/locate/tria

Early white matter microstructural alterations in cerebral small vessel disease: A tract-specific diffusion tensor imaging and cardio-cerebrovascular risk perspective

Zaw Myo Hein [a], Muhammad Danial Che Ramli [b], Usman Jaffer [c], Che Mohd Nasril Che Mohd Nassir [d,*]

[a] Department of Basic Medical Sciences, College of Medicine, Ajman University, P.O.BOX:346 Ajman, United Arab Emirates
[b] Department of Diagnostic and Allied Health Science, Faculty of Health and Life Sciences, Management and Science University, 40150, Shah Alam, Selangor, Malaysia
[c] Kulliyyah of Islamic Revealed Knowledge and Human Sciences, International Islamic University Malaysia, 50728, Kuala Lumpur, Malaysia
[d] Department of Anatomy and Physiology, School of Basic Medical Sciences, Faculty of Medicine, Universiti Sultan Zainal Abidin, 20400, Kuala Terengganu, Terengganu, Malaysia

ARTICLE INFO

Keywords:
Cerebral small vessel disease
White matter integrity
Diffusion tensor imaging
QRISK3
Microstructure

ABSTRACT

Background: Silent cerebral small vessel disease (CSVD), marked by white matter hyperintensities (WMHs), are commonly detected incidentally on neuroimaging. Emerging evidence links early brain microstructural changes to modifiable cardio-cerebrovascular risks, even without neurological symptoms. This study aimed to explore the relationship between cardio-cerebrovascular risk, white matter tract integrity, and cognitive performance in asymptomatic adults, using QRISK3 profiling, diffusion tensor imaging (DTI), and neurocognitive evaluation.
Methods: Sixty neurologically asymptomatic adults (mean age: 39.8 ± 11.5 years) with low to moderate QRISK3 scores underwent standardized neurocognitive assessment 3T brain MRI, including DTI sequences. Lesion-guided region-of-interest (ROI) tractography was used to assess six bilateral white matter tracts commonly affected in CSVD: the anterior and superior corona radiata and the superior longitudinal fasciculus (SLF).
Results: WMHs were identified in 20 individuals (33.3 %). Their presence was significantly associated with aging, systolic blood pressure, hypertension, and QRISK3 score ($p < 0.05$). While no significant cognitive impairment was observed, processing speed was negatively correlated with age and QRISK3. Although DTI metrics such as fractional anisotropy (FA) and mean diffusivity (MD) did not significantly differ across groups, tract-specific analysis revealed that higher QRISK3 scores were significantly associated with reduced white matter integrity in the left SLF.
Conclusion: These findings highlight the presence of early, subclinical white matter alterations in individuals at cardio-cerebrovascular risk, even in the absence of neurological symptoms. The integration of tract-specific DTI analysis with vascular risk profiling may provide a sensitive approach for detecting preclinical CSVD and guiding early intervention strategies in at-risk populations.

1. Introduction

Cerebral small vessel disease (CSVD) encompasses a spectrum of pathological, clinical, and radiological abnormalities linked to damage in the brain's microvasculature, particularly small penetrating arteries and arterioles (50–500 μm) that supply subcortical structures [1,2]. It is a major cause of parenchymal brain injury, most notably in deep white matter, and is frequently associated with pathology in distal leptomeningeal and intracerebral vessels [3]. CSVD represents one of the most prevalent neurological conditions in aging populations, with increasing incidence in developed societies [4,5].

Alarmingly, a hallmark of CSVD is the presence of so-called "silent" or asymptomatic lesions, such as white matter hyperintensities (WMHs) and silent brain infarcts, often detected incidentally through magnetic resonance imaging (MRI) [6,7]. On conventional T2-weighted MRI, WMHs appear as diffuse areas of hyperintensity, but these changes correlate only moderately with clinical parameters such as cognitive function [8,9]. This limited correlation highlights the need for more

* Corresponding author.
E-mail address: nasrilnassir@unisza.edu.my (C.M. Nasril Che Mohd Nassir).

https://doi.org/10.1016/j.tria.2025.100425
Received 20 June 2025; Received in revised form 10 July 2025; Accepted 19 July 2025
Available online 19 July 2025

sensitive imaging biomarkers to assess white matter integrity and disease progression. Besides, diffusion MRI (dMRI), particularly diffusion tensor imaging (DTI), offers a more refined approach for investigating early microstructural alterations in white matter i.e., subtle disruptions in axonal and myelin integrity that preceded the appearance of overt lesions such as WMHs visible on conventional MRI. These alterations can be detected through DTI, where it provides quantitative metrics such as fractional anisotropy (FA) and mean diffusivity (MD) which reflect white matter tract integrity and have shown stronger associations with cognitive impairments, especially in domains like executive function and processing speed [10–12].

To date, the pathophysiology of CSVD extends beyond vessel-specific alterations, involving systemic factors like chronic hypoperfusion, impaired cerebrovascular reactivity, and blood–brain barrier (BBB) dysfunction [13–16]. Yet, the influence of broader cardio-cerebrovascular risk profiles on white matter structure, particularly in asymptomatic individuals remains underexplored. QRISK3, is a cardiovascular risk prediction algorithm developed in the United Kingdom, which estimates 10-year risk of cardiovascular events by integrating multiple variables including age, sex, ethnicity, systolic blood pressure, total cholesterol/high density lipoprotein (HDL) ratio, smoking status, diabetes, chronic kidney disease, atrial fibrillation, rheumatoid arthritis, and other comorbidities. [17–19]. While originally designed to predict cardiovascular events, its inclusion of diverse vascular and metabolic factors makes it potentially relevant for assessing cerebrovascular risk and early microvascular dysfunction in the brain. Its potential relevance as a proxy for cerebral microvascular vulnerability warrants investigation in the context of CSVD.

Hence, this study aims to address the critical need for early biomarkers of CSVD by examining the associations between cardio-cerebrovascular risk (as measured by QRISK3), white matter microstructural integrity (via DTI), and cognitive performance in a cohort of asymptomatic individuals. By integrating vascular risk assessments with advanced neuroimaging and comprehensive cognitive testing, we aim to identify subtle, tract-specific white matter changes that may precede the onset of overt clinical symptoms.

Finally, from an anatomical standpoint, this work contributes to the mapping of vascular risk-related vulnerabilities across specific white matter tracts. Understanding these relationships not only enhances the anatomical framework of CSVD progression but also provides insight into the neural substrates underlying early cognitive decline. Ultimately, such findings could guide targeted interventions aimed at preserving white matter health and mitigating long-term cognitive consequences.

2. Materials and methods

2.1. Ethics approval, sample size estimation, and subject recruitment

This study was conducted at Hospital Universiti Sains Malaysia (HUSM), a tertiary referral center for neurological disorders located on the east coast of Peninsular Malaysia, serving a catchment population of over four million. Ethical approval was granted by the Human Research Ethics Committee of Universiti Sains Malaysia (USM/JEPeM/15030096).

Participant recruitment was carried out using convenience sampling from individuals attending routine medical follow-up appointments at the Family Medicine Clinic, HUSM. Prior to inclusion, demographic data (age, sex, and race) and clinical variables (smoking status, diabetes status, body mass index, and systolic blood pressure) were recorded. These parameters were subsequently used to compute individual cardiocerebrovascular risk scores using the QRISK3 algorithm.

Sample size was estimated based on the ability to detect a moderate correlation ($r = 0.35$) between QRISK3 scores and DTI metrics such as FA or MD, in line with previous studies assessing vascular risk and neuroimaging (i.e., white matter microstructure) [20,21]. Using a two-tailed test, an alpha level of 0.05, and 80 % power, the required sample size to detect this effect was calculated to be 58 subjects. The bivariate normal model was used, and calculation was performed using G*Power version 3.1.9.7. To account for potential data loss or poor-quality imaging, we recruited 60 subjects. This sample size is also adequate for multiple linear regression analyses involving up to 5 predictors, maintaining a subject-to-variable ratio above the recommended minimum of 10:1 [21,22].

2.2. Cardio-cerebrovascular risk assessment

Cardio-cerebrovascular risk was assessed using the QRISK3 (2018) online calculator (http://www.qrisk.org/index.php), developed by the University of Nottingham and EMIS. This tool estimates the 10-year risk of developing cardiovascular disease based on demographic and clinical variables. Risk categories were defined as follows: low ($\leq$10 %), moderate (10.1–20 %), and high ($\geq$20.1 %) [23]. Eligible subjects were asymptomatic individuals aged 25–62 years, with no history of neurological disease and classified as having low to moderate cardiovascular risk based on their QRISK2 scores.

Individuals with high cardiovascular risk ($\geq$20.1 %) or any prior neurological diagnosis were excluded from the study. They were excluded to minimize potential confounding from established or subclinical cerebrovascular pathology that could independently influence white matter integrity and cognitive performance. The primary aim of this study was to investigate early subclinical brain microstructural changes associated with low to moderate cardio-cerebrovascular risk in an asymptomatic population. Including high-risk individuals could obscure subtle associations due to a higher likelihood of existing vascular burden, previous silent infarcts, or preclinical neurodegenerative processes [24]. This exclusion criterion ensures a more homogenous sample, enhancing the sensitivity of detecting early imaging biomarkers relevant to CSVD prevention and risk stratification.

2.3. Neurocognitive assessment

Cognitive performance was assessed using the Wechsler Adult Intelligence Scale – Fourth Edition (WAIS-IV), a standardized tool for evaluating intellectual and memory functions [25]. Three composite indices were analyzed to capture distinct cognitive domains relevant to white matter integrity: (a) The perceptual reasoning index (PRI), which assesses nonverbal reasoning and visuospatial problem-solving, was derived from three subtests: Block design, matrix reasoning, and visual puzzles; (b) the working memory index (WMI), reflecting attention, mental manipulation, and sequential processing, was obtained through the digit span and letter–number sequencing subtests; (c) the processing speed index (PSI), which evaluates the speed of visual information processing and graphomotor coordination, was calculated from the coding and symbol Search subtests. Subtest scores from each index were used for multimodal analyses to explore associations with white matter integrity and cardio-cerebrovascular risk.

2.4. Diffusion MRI protocols

A Philips Achieva (Best, The Netherlands) 3T MRI machine with a 32-channel head coil (b-value: 1000 s/mm^2) was used for brain scanning with the following acquisition parameters: For structural image acquisition 3D-T1, echo time (TE)/repetition time (TR) = 10/678 ms, reconstruction matrix = 512 × 512 × 40, field of view (FOV) = 230 mm, voxel size = 0.45 mm × 0.45 mm, slice spacing = 0 mm, slice thickness = 2.5 mm, flip angle = 70, and 180 contiguous sagittal slices orientation; for T2, TE/TR = 80/3000 ms, reconstruction matrix = 512 × 512 × 24, FOV = 230 mm, voxel size = 0.45 × 0.45, slice spacing = 1.0 mm, slice thickness = 2.5 mm, and flip angle = 90; for 3D-fluid attenuated inversion recovery (FLAIR), TE/TR = 125/11,000 ms, TI = 2800 ms, reconstruction matrix = 512 × 512 × 24, FOV = 230 mm, voxel size = 0.45 mm × 0.45 mm, slice spacing = 0 mm, slice thickness = 2.5 mm,

flip angle = 90, and 170 contiguous sagittal slices orientation; and for DTI, a scheme of 32 directions with a b-value of 1000 s/mm^2, TE/TR = 72/6951 ms, reconstruction matrix = 96 × 96, FOV = 240 mm, voxel sizes = 2.5 mm × 2.5 mm, slice spacing = 0 mm, slice thickness = 2.5 mm, and flip angle 90. The total scanner time was 15–20 min, per the subject's ability.

2.5. Image analysis and evaluation of WMHs

WMHs were topographically classified into periventricular and deep WMHs, based on their anatomical location. Identification and differentiation were made by assessing MRI signal characteristics hyperintense on T2-weighted and FLAIR sequences (most reliably on FLAIR), and hypointense on T1-weighted sequences as well as lesion size, shape, border definition, and location, in accordance with previously established radiological criteria and the STRIVE guidelines [8].

Two experienced neuroradiologists, blinded to all clinical data, independently assessed the presence and severity of WMHs using the Fazekas scale [26,27]. To assess reliability, intra- and inter-rater agreement analyses were conducted on a random sample of 60 subjects, with re-evaluations performed after an interval of over one month. The inter-rater agreement yielded kappa (κ) values of 0.96 (95 % CI: 0.80–1.00; $p < 0.05$) for deep WMHs and 0.86 (95 % CI: 0.70–1.00; $p < 0.05$) for cases with both periventricular and deep WMHs. Intra-rater reliability was similarly high, with κ = 0.95 and κ = 0.90, respectively, indicating excellent consistency.

Initial manual assessments were performed using MeVisLab Diffusion Imaging in Radiology (MeDInria) software version 2.2 (Inria, National Institute for Research in Digital Science and Technology, France) [28]. To enhance objectivity and quantify WMHs burden, automated lesion detection and segmentation were conducted using the Lesion Segmentation Tool (LST) implemented in SPM12 (Wellcome Centre for Human Neuroimaging, UCL), executed through MATLAB version R2024b (MathWorks, Natick, MA, USA). The lesion growth algorithm (LGA), with a threshold κ = 0.15, was used for segmenting and calculating WMH volume and lesion count [29].

Based on MRI findings, subjects were categorized into two groups: (1) asymptomatic individuals with normal-appearing white matter (no WMHs), and (2) asymptomatic individuals presenting with WMHs. Quantification of lesion count and volume followed validated methods to ensure consistency and accuracy in WMHs burden assessment.

2.6. Region of Interest Analysis (ROI) and tractography

White matter tractography analysis was conducted using DSI Studio (http://dsi-studio.labsolver.org) for both subjects with WMHs and those without. A DTI reconstruction scheme was employed, with 32 diffusion sampling directions acquired at a *b*-value of 1000 s/mm^2. The in-plane resolution was set at 2.5 mm, with a matching slice thickness of 2.5 mm. DTI preprocessing and tensor estimation were performed to enable quantitative evaluation of white matter microstructural integrity.

Using anatomical references from FLAIR images, a voxel-based ROI approach was applied to WMHs identified in the axial plane, followed by regional tractography. Deterministic fiber tracking was conducted using a validated algorithm in DSI Studio, with whole brain seeding [30]. The tracking parameters included an angular threshold of 60°, a step size of 1.25 mm, and an automatically determined anisotropy threshold. Tracks shorter than 30 mm were excluded, and 5000 seeds were generated per subject to ensure robust fiber reconstruction.

The white matter tracts associated with WMHs were anatomically defined using the Johns Hopkins University (JHU) ICBM-DTI-81 white matter atlas, embedded in DSI Studio. This allowed for the identification and classification of tract involvement based on standardized neuroanatomical labels. Tract-specific subgroup analyses were based on the spatial distribution of WMHs. Only subjects whose WMHs were localized to a specific tract (e.g., anterior corona radiata, superior longitudinal fasciculus) were included in the corresponding tract-based diffusion analysis. As a result, the number of subjects analyzed per tract varied depending on lesion location. To enable group comparisons, the same anatomical regions were reconstructed in subjects without WMHs using the same atlas-based ROI placement strategy. This approach ensured anatomical consistency while focusing the analysis on regions directly affected by WMH. Moreover, each tract-specific sample size reflects the number of individual tracts reconstructed across subjects. Some participants contributed more than one tract to the analysis if they had WMHs in multiple tracts or bilaterally. Therefore, the total number of reconstructed tracts does not equal the number of unique subjects. The maximum number of subjects contributing to tract-specific analyses did not exceed 20, corresponding to the group with WMHs.

Within each identified tract, quantitative DTI metrics, including FA and MD, were extracted. These metrics were averaged over the reconstructed tract volumes, allowing for assessment of microstructural integrity and comparison between groups. This tract-based analysis enabled a focused investigation into whether subtle microstructural changes occur in anatomically vulnerable pathways, even in the absence of radiologically apparent lesions, thus supporting the study's aim of identifying early CSVD-related changes.

2.7. Statistical data analysis

All statistical analyses were performed using Statistical Package for Social Sciences (SPSS) version 26.0 (IBM Corp., Armonk, NY, USA). A significance level of α = 0.05 was applied, with a 95 % confidence interval (CI). Descriptive statistics, including means, standard deviations, medians, and interquartile ranges (IQR), were computed to summarize demographic and clinical data. Pearson's correlation was used to assess linear relationships between continuous variables. Group comparisons were conducted using the independent sample *t*-test for normally distributed data and the chi-square (χ^2) test for categorical variables. For data not normally distributed, appropriate non-parametric tests were applied as needed.

To visualize the interaction between continuous variables, a contour plot analysis was performed using MINITAB version 17 (Minitab, LLC, State College, PA, USA), illustrating the relationship between one or more response variables and a set of quantitative predictors [31]. Multiple linear regression and logistic regression models were used to explore associations among age, QRISK3 scores, neurocognitive performance, and DTI metrics. All models were adjusted for relevant covariates, including sex, ethnicity, and established cardiocerebrovascular risk factors. Further regression analyses were performed to examine the relationships between tract-specific DTI parameters (e.g., FA and MD values) and predictor variables (age, QRISK2 score, cognitive indices), also controlling demographic and clinical covariates.

3. Results

3.1. Demographic and clinical characteristics of study subjects according to WMHs status

Table 1 presents the demographic, clinical, and cognitive profiles of the 60 asymptomatic subjects, stratified by the presence (n = 20) and absence (n = 40) of WMHs. Subjects in the WMHs group were significantly older than those in the group with absence of WMHs (46.6 ± 12.2 vs. 36.0 ± 9.6 years, $p < 0.001$), with higher systolic blood pressure (SBP) (141.3 ± 16.6 mmHg vs. 122.8 ± 10.4 mmHg, $p < 0.001$), and significantly elevated QRISK3 scores (6.07 ± 6.7 % vs. 1.20 ± 1.4 %, $p < 0.001$). Hypertension was also more prevalent in the WMHs group (30.0 % vs. 7.5 %, p = 0.02). No significant differences were found in sex, ethnicity, educational level, smoking status, body mass index (BMI), cholesterol-to-HDL ratio, or other vascular risk factors such as diabetes, atrial fibrillation, or hyperlipidemia.

Although the WMHs group showed a numerically higher proportion

Table 1
Demographics and characteristics of the study subjects.

Variables	Total (n = 60)	WMHs		
		Present (n = 20)	Absent (n = 40)	*p*-value
Age, yrs*	39.60 ± 11.60	46.60 ± 12.2	36.0 ± 9.6	***p*<0.001**[#]
Sex, n (%)				0.841
Male	19 (31.7)	8 (40.0)	11 (27.5)	
Female	41 (68.3)	12 (60.0)	29 (72.5)	
Ethnicity, n (%)				0.190
Malay	54 (90)	18 (90.0)	36 (90.0)	
Chinese	4 (6.7)	1 (5.0)	3 (7.5)	
Others	2 (3.3)	1 (5.0)	1 (2.5)	
Education level, n (%)				0.306
Low[a]	5 (8.3)	1 (5.0)	4 (10.0)	
Intermediate[b]	27 (45)	12 (60.0)	15 (37.5)	
High[c]	28 (46.7)	7 (35.0)	21 (52.5)	
Smoking, n (%)				0.374
Non-smoker	52 (86.6)	16 (80.0)	36 (90.0)	
Ex-smoker	6 (10)	3 (15.0)	3 (7.5)	
Light smoker	1 (1.7)	0 (0)	1 (2.5)	
Moderate smoker	1 (1.7)	1 (5.0)	0 (0)	
Heavy smoker	0 (0)	0 (0)	0 (0)	
Type 2 Diabetes, n (%)	0 (0)	0 (0)	0 (0)	–
Family History[d], n (%)	15 (25)	12 (60.0)	3 (7.5)	0.264
Atrial fibrillation, n (%)	0 (0)	0 (0)	0 (0)	–
Hyperlipidemia, n (%)	0 (0)	0 (0)	0 (0)	–
Hypertension, n (%)	9 (25)	6 (30.0)	3 (7.5)	**0.020** [#]
CHO to HDL ratio *	3.88 ± 0.99	3.62 ± 0.63	4.01 ± 1.12	0.200
SBP (mmHg) *	128.9 ± 15.4	141.3 ± 16.6	122.8 ± 10.4	***p*<0.001**[#]
BMI (kg/m^2) *	24.7 ± 4.4	25.8 ± 3.5	24.2 ± 4.7	0.20
QRISK3 score (%) *	2.83 ± 4.42	6.07 ± 6.7	1.20 ± 1.4	***p*<0.001**[#]
WAIS-IV Indices *				
PRI	102.9 ± 12.9	100.8 ± 10.9	103.0 ± 13.9	0.571
WMI	108.5 ± 19.1	107.3 ± 13.1	108.1 ± 19.9	0.933
PSI	103.7 ± 13.9	98.6 ± 12.0	103.7 ± 14.6	0.210

Note: data values are presented as number of subjects (n), with percentage (%) in parentheses; light smoker (≤10) ; Moderate smoker (10–19) ; Heavy smoker (≥20) ; * Data are means ± standard deviations; [a] None, primary or secondary education; [b] Higher secondary or vocational; [c] university or higher professional education; [d] Angina or heart attack in a 1st degree relative <60 years of age, n (%). Subgroups according to the presence or absence of white matter hyperintensities (WMHs) were compared using the χ^2 test and the independent sample *t*-test. [#]p = significant difference [2-tailed] at the <0.05 level). BMI, body mass index; CHO, Cholesterol; HDL, High-Density Lipoprotein; PRI, Perceptual Reasoning Index; PSI, Processing Speed Index; SBP, Systolic Blood Pressure; WAIS-IV, Weschler Adult Intelligence Scale Version IV; WMI, Working Memory Index.

of individuals with a family history of cardiovascular disease (60.0 % vs. 7.5 %), this difference did not reach statistical significance ($p = 0.26 > 0.05$), possibly due to the small sample size. Moreover, neurocognitive performance, as measured by the WAIS-IV indices, also did not differ significantly between groups. However, a trend toward lower scores in the PSI was observed in the WMHs group (98.6 ± 12.0 vs. 103.7 ± 14.6, $p = 0.21 > 0.05$), suggesting potential early functional impact associated with WMHs. These findings highlight the relationship between elevated cardiocerebrovascular risk and the presence of WMHs, even in an asymptomatic, community-based population.

3.2. WMHs profiles

As summarized in Table 1, a total of 20 subjects (33 %; mean age: 46.6 ± 12.2 years) were identified as having WMHs. Notably, the median lesion volume and lesion count were 0.00 mL and 0, respectively, because over 50 % of participants did not have any detectable WMHs. However, the interquartile ranges extend above zero (interquartile range [IQR]: 0.00–0.16 mL), with 25 % of subjects exhibiting lesion volumes equal to or greater than 1 mL, reflecting the distribution of lesion burden in those with WMHs. This statistical pattern is common in datasets with a substantial proportion of zero values and a skewed distribution among positive cases. Moreover, the median number of WMH lesions was 0 (IQR: 0–4); in over half of the subjects with WMHs, the total lesion count was ≥1. Regarding severity, 12 subjects (55.6 %) were rated as Fazekas scale 2, while 8 (44.4 %) were classified as Fazekas scale 1. The spatial distribution of WMHs is illustrated in Fig. 1. All subjects with WMHs demonstrated deep WMHs, located in subcortical white matter distant from the lateral ventricles. Additionally, 13 subjects (72.2 %) exhibited a mixed pattern, with both deep and periventricular WMHs, whereas none had isolated periventricular lesions.

3.3. Risk factors associated with the presence of WMHs

The characteristics of subjects with and without WMHs are listed in Table 1. The association was corrected for multivariable non-collinearity. The model fit assessment was performed using the Hosmer-Lemeshow goodness-of-fit test, fitted for age and QRISK3 ($p > 0.05$). Therefore, we found that age had a linear association with QRISK3 score (standardized β coefficients, 0.75 [95 % CI: 1.44 to 2.36], $p < 0.05$), hence, increased subjects' age will have a higher QRISK3 score (see contour plot in Fig. 1F). After adjusting covariates such as sex and age, the presence of WMHs was significantly increased with age (odd ratio [OR] per standard error, 0.91; 95 % CI: 0.86 to 0.97) and was more prevalent in subjects with higher QRISK3 score (OR, 0.65; 95 % CI: 0.48 to 0.88). WMHs are also associated with cardio-cerebrovascular risk factors such as hypertension and an increase in SBP (see Table 2).

Based on Table 1, subjects with WMHs demonstrated lower neurocognitive performance after adjusting for covariates including age and QRISK3 scores; however, these differences were not statistically significant. Notably, PSI showed a significant negative linear association with age (standardized $\beta = -0.55$, 95 % CI: −0.94 to −0.38, $p < 0.05$) and also QRISK3 score (standardized $\beta = -0.37$, 95 % CI: −1.91 to −0.34, $p < 0.05$), indicating that increased age and higher cardio-cerebrovascular risk were associated with reduced processing speed performance. This relationship is further visualized in the contour plots in Fig. 1(F and G). However, as shown in Table 2, the presence of WMHs was not significantly associated with increased odds of reduced neurocognitive performance across the measured cognitive domains.

3.4. Cerebral white matter microstructural integrity

Three bilateral white matter tracts such as the ACR, superior corona radiata (SCR), and SLF were selected for analysis based on the frequency and distribution of WMHs observed in the MRI scans of study subjects. This yielded a total of six tract-specific ROIs: right ACR (RACR, n = 7), left ACR (LACR, n = 7), right SCR (RSCR, n = 4), left SCR (LSCR, n = 4), right SLF (RSLF, n = 5), and left SLF (LSLF, n = 3) (see Fig. 2).

White matter integrity was assessed using DTI parameters, whereby subjects with WMHs exhibited lower FA and higher MD across all selected tracts compared to those without WMHs, although these differences did not reach statistical significance (see Table 3). Similarly, axial diffusivity (AD) and radial diffusivity (RD) values varied between groups but were not significantly different from one another.

Correlation analysis revealed that FA was negatively associated with age and QRISK3 score (low to moderate strength), while AD showed a weak negative correlation with age (Table 4). However, no significant

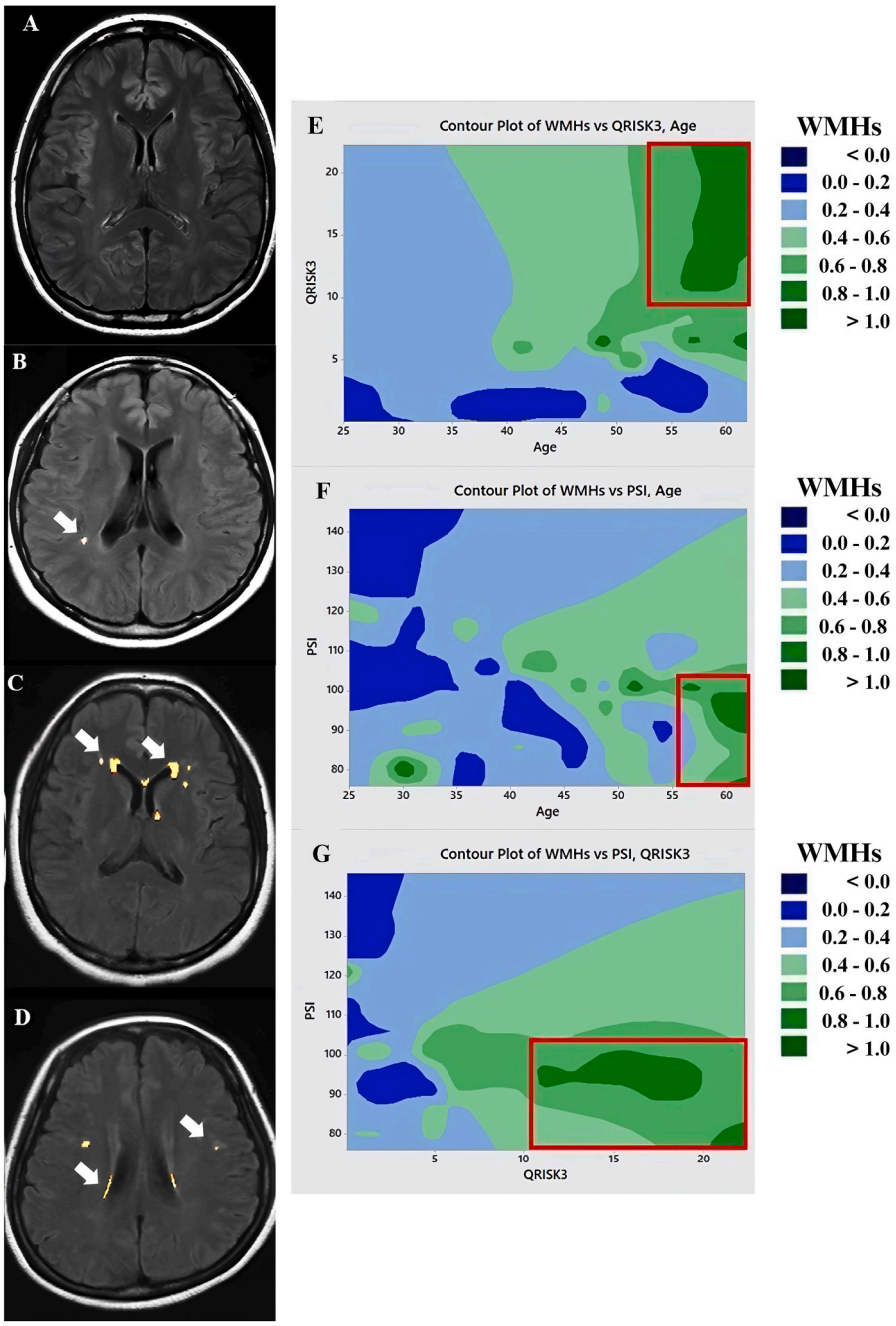

Fig. 1. Left column (A–D): Spatial distribution of white matter hyperintensities (WMHs) on fluid attenuated inversion recovery (FLAIR) images using the lesion segmentation tool (LST) with the lesion growth algorithm (LGA). Bright yellow overlays indicate statistically probable WMH voxels. (A) A normal brain scan without WMHs. (B) A case showing isolated deep WMHs (white arrows). (C–D) Cases showing both periventricular and deep WMHs (white arrows). Right column (E–G): Contour plots illustrating the relationship between WMHs, QRISK3 score, age, and Processing Speed Index (PSI). (E) WMHs plotted against age and QRISK3 score. The red box (dark green region) highlights increased WMH burden in individuals aged >55 years with QRISK3 scores ≥10 %. (F) WMHs plotted against age and PSI. The red box shows that individuals aged >55 years with lower PSI scores (≤110) exhibit increased WMH burden. (G) WMHs plotted against QRISK3 and PSI. The red box indicates that subjects with higher QRISK3 scores (≥10 %) and lower PSI scores (≤110) are more likely to have a greater WMHs load.

associations between these DTI metrics and age or QRISK3 were confirmed in further regression analysis. Notably, a linear regression model identified a significant association between QRISK3 score and all four diffusion parameters (FA, MD, AD, RD) in the left SLF (LSLF). Additionally, FA in most of the selected tracts showed a positive, albeit non-significant, correlation with cognitive performance across all WAIS-IV indices (PRI, WMI, and PSI) (Table 4). MD and RD were not significantly correlated with any cognitive domain, while AD showed a positive correlation with PRI only. These findings indicate that, in this cohort, DTI-derived measures of white matter integrity were not significantly associated with neurocognitive performance, although trends in FA suggest potential functional relevance.

4. Discussion

This study provides novel insights into early white matter microstructural changes associated with CSVD in an asymptomatic, community-based population. Our findings demonstrate that WMHs and associated DTI alterations can be detected even in relatively young individuals with low to moderate QRISK3 scores, emphasizing the silent

Table 2
Association between potential risk factors and presence of white matter hyperintensities (WMHs).

Risk factors	WMHs	
	Present (n = 20) versus absent (n = 40)	
	Multiple Logistic Regression[a]	
	OR (95 % CI)	*p*-value
Age[b]	0.91 (0.86–0.97)	**0.03**[e]
Family History[c]	2.07 (0.58–7.46)	0.261
Hypertension	5.50 (1.19–25.54)	**0.03**[e]
Systolic blood pressure (SBP)[d]	0.89 (0.83–0.95)	***p*<0.001**[e]
Body mass index (BMI)	0.92 (0.80–1.05)	0.20
QRISK3 Score	0.65 (0.48–0.88)	***p*<0.001**[e]
WAIS-IV PRI	1.01 (0.94–1.08)	0.882
WAIS-IV WMI	0.98 (0.93–1.03)	0.400
WAIS-IV PSI	1.04 (0.98–1.11)	0.163

CI, confidence interval; ePVS, enlarged perivascular spaces; OR, odds ratio; PRI, perceptual reasoning index; PSI, processing speed index; WAIS, Weschler Adult Intelligence Scale version IV; WMI, working memory index;.

[a] Adjusted for age and gender;.
[b] per one-year;.
[c] Angina or heart attack in a 1st degree relative <60 years of age;.
[d] per mmHg;.
[e] p = significant difference (2-tailed) at 0.05 level.

and progressive nature of CSVD. Notably, increased age, SBP, hypertension, and QRISK3 scores were significantly associated with the presence of WMHs. While cognitive scores did not significantly differ between groups, lower processing speed was linked to both higher age and QRISK3 scores, suggesting early functional vulnerability despite subclinical presentation.

4.1. White matter microstructural alterations in CSVD: A DTI and neuroanatomical perspective

Our tract-based DTI analysis offers a neuroanatomically grounded perspective on early white matter changes in CSVD. Furthermore, advanced DTI metrics including: (1) FA, where lower values indicate reduced fiber integrity due to axonal or myelin damage [32,33]; (2) MD, with higher values reflecting increased extracellular water diffusion, often associated with tissue degeneration [34]; (3) AD RD, which respectively reflect diffusion along and perpendicular to the axonal axis and provide insights into axonal and myelin integrity [35,36]. These parameters may offer pathophysiological insight, for example, increases in RD have been linked to demyelination, whereas reductions in AD may reflect axonal degeneration [37,38].

We focused on three bilateral white matter tracts, such as the ACR, SCR, and SLF, selected based on the spatial overlap with WMHs identified through lesion segmentation. These tracts represent major projection and association fibers critical for cognitive processing, attention, executive function, and sensorimotor integration, and are known to be highly vulnerable to microvascular injury due to their distal perfusion territory and high myelin content [39,40].

The anterior and superior corona radiata are projection fibers involved in the relay of information between cortical and subcortical structures. Damage to these fibers has been previously associated with declines in motor coordination, processing speed, and working memory hallmarks of early vascular cognitive impairment [41,42]. The SLF, a major association pathway linking the frontal, parietal, and temporal lobes, plays a key role in language, attention, and working memory [43]. In particular, our finding that QRISK3 was significantly associated with lower FA and higher MD in the left SLF (LSLF) points to this tract as a region of early vulnerability to subclinical vascular burden.

Importantly, our ROI-based tractography approach, guided by WMHs lesion location, provides greater anatomical specificity than whole-brain voxel-based analyses or conventional region-of-interest placement. While voxel-wise approaches such as tract-based spatial statistics (TBSS) provide robust whole-brain comparisons, they may average over heterogeneous tract segments and miss localized changes that reflect early pathology [44,45]. Our method allowed us to detect subtle tract-specific alterations within a framework that respects both structural and functional connectivity.

From a neuroimaging methods standpoint, DTI offers unique sensitivity to the integrity of white matter microstructure by quantifying direction-dependent water diffusion. Compared to conventional MRI, which primarily detects gross tissue changes (e.g., WMHs or infarcts), DTI reveals microstructural disruptions in axonal membranes, myelin sheaths, and extracellular space changes that often precede the appearance of visible WMHs. When compared to other neuroimaging modalities, T2-weighted and FLAIR MRI are sensitive to WMHs but limited in quantifying subtle changes and distinguishing lesion severity [8]. Magnetization transfer imaging (MTI) and myelin water imaging (MWI) are more specific to myelin integrity but are less widely available and technically demanding [46,47]. Besides, quantitative susceptibility mapping (QSM) and arterial spin labeling (ASL) provide insight into iron content and perfusion deficits, respectively, but do not directly characterize fiber microstructure [48,49]. In contrast, DTI provides a practical, widely available, and non-invasive technique for *in vivo* white matter assessment with strong anatomical resolution, particularly when combined with tractography [50,51].

Our findings are consistent with postmortem and histological studies, which have documented white matter rarefaction, arteriolosclerosis, and demyelination in regions corresponding to the ACR and SLF in patients with CSVD [52,53]. Histopathology has shown that these changes may occur even in the brains of individuals without clinically manifest stroke or dementia, supporting our assertion that microstructural damage precedes functional decline [54–56]. Studies combining DTI with postmortem validation have confirmed that decreased FA correlates with demyelination and axonal loss, and that MD correlates with increased extracellular fluid due to gliosis and perivascular edema [57,58].

Therefore, the current study strengthens the evidence that DTI-based tract analysis can serve as a sensitive biomarker of preclinical CSVD. The identification of tract-specific associations with vascular risk profiles, particularly QRISK3, adds a clinically actionable layer, potentially guiding early preventive strategies in midlife populations.

4.2. Cognitive function and white matter integrity: early functional signatures of vascular risk

Although cognitive performance did not significantly differ between subjects with and without WMHs, our findings suggest early and functionally relevant changes in processing speed that may precede overt cognitive impairment. In particular, the PSI demonstrated a significant negative correlation with age and QRISK3 score, reinforcing its sensitivity as a marker of early cerebrovascular compromise. This aligns with previous research identifying processing speed as one of the earliest cognitive domains affected in CSVD, even before memory or executive dysfunction becomes apparent [59,60].

Processing speed relies on efficient communication across distributed neural networks, particularly within frontoparietal white matter tracts, which include the corona radiata and SLF [61,62], precisely the tracts examined in this study. Subtle disruptions in these pathways, as reflected in reduced FA, may lead to inefficient signal conduction and slower information processing, even in the absence of a gross lesion burden. The correlations observed between FA values and all three WAIS-IV indices i.e., PRI, WMI, and PSI though not statistically significant, were directionally consistent with prior DTI literature. FA has been shown to positively correlate with processing speed and working memory in both healthy aging populations and patients with vascular cognitive impairment [63,64]. This supports the hypothesis that white matter tract integrity underlies cognitive performance, particularly in

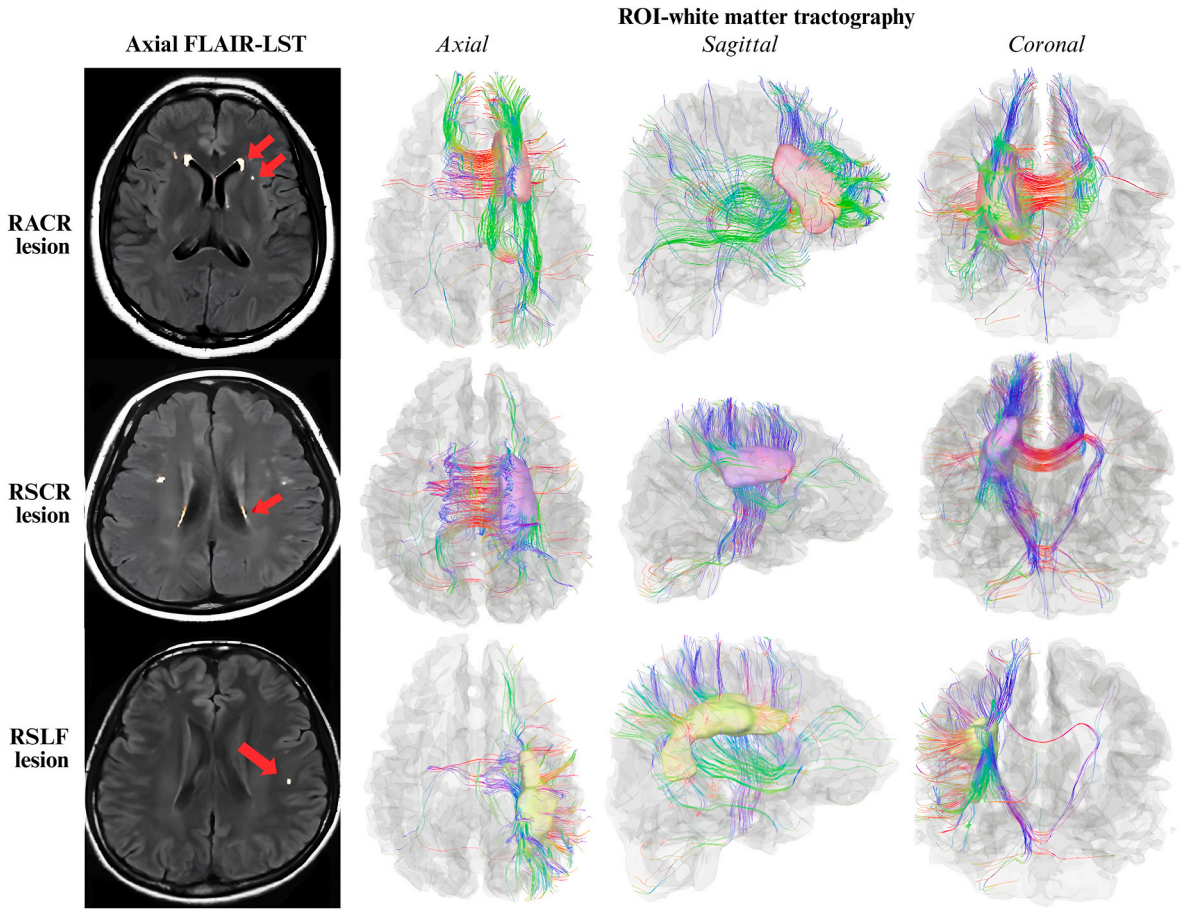

Fig. 2. From left: the first rows show axial fluid attenuated inversion recovery (FLAIR) images with white matter hyperintensities (WMHs) voxel outputs from the lesion segmentation tool (LST) (axial FLAIR-LST) showing right anterior corona radiata (RACR) lesion (red arrow) and RACR tractography (axial, sagittal and coronal-rostral view). The second rows show FLAIR images with WMHs voxel outputs from the LST showing the right superior corona radiata (RSCR) lesion (red arrow) and RSCR tractography (axial, sagittal and coronal-rostral view). The third row shows FLAIR images with WMHs voxel outputs from the LST showing right superior longitudinal fasciculus (RSLF) lesion (red arrow) and RSLF tractography (axial, sagittal and coronal-rostral view). The blue, red, and green colors on the second and third rows of the figures represent white matter fibers running along the inferior–superior, right–left, and anterior–posterior orientations, respectively. Notes: LST followed the native Statistical Parametric Mapping (SPM) and Matrix Laboratory (MATLAB) orientations for producing JPEG images; hence, the original radiological view (left on right) obtained from the magnetic resonance imaging (MRI) scanner was shifted to neurological view (right on right) as a reminder of viewing interpretation. FLAIR, fluid-attenuated inverse recovery; RACR, right anterior corona radiata; RSLF, right superior longitudinal fasciculus; RSCR, right superior corona radiata; ROI, region of interest.

domains that depend on rapid, coordinated interregional communication.

Interestingly, while MD, AD, and RD showed little to no relationship with cognitive scores, FA consistently demonstrated stronger correlations. This may be due to FA's higher sensitivity to anisotropic water diffusion, which is disrupted by both demyelination and axonal damage processes common in early CSVD [65]. It is possible that MD, AD, and RD reflect later-stage or more regionally diffuse pathology that has not yet manifested in our asymptomatic sample. The left SLF (LSLF) again emerged as the most consistently implicated tract, linking vascular risk (QRISK3), white matter changes (lower FA/higher MD), and PSI, further highlighting its importance in early CSVD-related cognitive changes. Collectively, these findings provide evidence that tract-specific microstructural degradation particularly within the LSLF may precede and predict decline in processing speed, serving as a potential biomarker of early CSVD-related cognitive vulnerability.

4.3. Integrating vascular risk, tract-specific imaging, and cognitive function

This study introduces a novel and clinically relevant framework that integrates cardio-cerebrovascular risk profiling (QRISK3), tract-specific DTI analysis, and neurocognitive assessment to investigate early CSVD pathology in an asymptomatic, middle-aged population. Most prior studies on CSVD have been conducted in older adults or individuals with clinically manifest cognitive impairment [66,67]. In contrast, our study of population i.e., free of stroke, dementia, or significant comorbidities demonstrates that white matter changes and early cognitive slowing can be detected well before clinical symptoms emerge.

One of the most innovative aspects of this study's approach is the use of WMH-guided ROI tractography, targeting specific fiber pathways based on lesion location rather than relying solely on generic templates or whole-brain statistics. This method allows for precise anatomical localization of microstructural changes and provides more direct insight into the functional implications of lesion topography [50,51]. The finding that higher QRISK3 scores are significantly associated with reduced FA and increased MD specifically in the LSLF provides both pathophysiological insight and translational relevance.

Moreover, QRISK3 has begun to be widely used in clinical settings to assess cardiovascular risk, yet its potential role as a proxy for cerebrovascular health has not been thoroughly investigated [17–19]. This study's findings suggest that even modest increases in QRISK3 below clinical thresholds for intervention may already be associated with cerebral white matter disruption, particularly in tracts involved in

Table 3
Comparison of the integrity of selected white matter between subjects with and without white matter hyperintensities (WMHs).

Tract parameters	(Mean ±_SD)		T-Statistics (df)	*p*-Value
	Without WMHs	With WMHs		
RACR				
FA	0.42 ± 0.03	0.42 ± 0.03	0.35 (37.94)	0.727
MD	0.82 ± 0.07	0.84 ± 0.08	−0.59 (33.83)	0.560
AD	1.23 ± 0.13	1.24 ± 0.14	−0.34 (35.39)	0.733
RD	0.63 ± 0.05	0.64 ± 0.06	−0.86 (32.21)	0.395
LACR				
FA	0.42 ± 0.02	0.42 ± 0.27	0.45 (34.42)	0.649
MD	0.82 ± 0.08	0.83 ± 0.08	−0.24 (38.36)	0.812
AD	1.23 ± 0.13	1.23 ± 0.13	−0.05 (38.38)	0.957
RD	0.62 ± 0.05	0.63 ± 0.05	−0.46 (37.81)	0.645
RSCR				
FA	0.46 ± 0.03	0.46 ± 0.02	−0.06 (48.00)	0.955
MD	0.81 ± 0.07	0.81 ± 0.07	−0.05 (37.40)	0.958
AD	1.26 ± 0.13	1.26 ± 0.12	−0.02 (40.09)	0.987
RD	0.59 ± 0.04	0.59 ± 0.05	−0.09 (34.21)	0.923
LSCR				
FA	0.46 ± 0.02	0.46 ± 0.02	0.17 (41.85)	0.866
MD	0.82 ± 0.07	0.83 ± 0.08	−0.30 (34.89)	0.765
AD	1.26 ± 0.12	1.27 ± 0.13	−0.16 (36.26)	0.875
RD	0.59 ± 0.05	0.60 ± 0.06	−0.45 (33.64)	0.655
RSLF				
FA	0.40 ± 0.02	0.40 ± 0.03	0.68 (34.32)	0.499
MD	0.77 ± 0.07	0.78 ± 0.08	−0.24 (34.15)	0.813
AD	1.13 ± 0.11	1.14 ± 0.12	−0.00 (35.76)	0.998
RD	0.59 ± 0.05	0.60 ± 0.06	−0.49 (32.15)	0.627
LSLF				
FA	0.41 ± 0.02	0.41 ± 0.03	0.94 (34.30)	0.355
MD	0.78 ± 0.07	0.78 ± 0.08	−0.13 (33.43)	0.897
AD	1.15 ± 0.11	1.15 ± 0.12	0.14 (34.98)	0.892
RD	0.59 ± 0.05	0.60 ± 0.06	−0.41 (31.77)	0.683

Notes: AD, axial diffusivity; FA, fractional anisotropy; LACR, left anterior corona radiata; LSCR, left superior corona radiata; LSLF, left superior longitudinal fasciculus; MD, mean diffusivity; RACR, right anterior corona radiata; RD, radial diffusivity; RSCR, right superior corona radiata; RSLF, right superior longitudinal fasciculus; WMH, white matter hyperintensity, p = significant difference.

cognitive efficiency. This positions QRISK3 as a valuable early risk stratification tool not only for cardiovascular events but also for preclinical CSVD.

Furthermore, the demonstration of tract-specific vulnerability (e.g., LSLF) in association with vascular risk adds to the growing body of evidence that CSVD is not merely diffuse and global but may target specific white matter circuits depending on vascular architecture, perfusion dynamics, and metabolic demand. This tract-based vulnerability framework may help identify early therapeutic targets and monitor treatment response in future preventive trials [68,69]. In summary, this study provides new evidence that bridges systemic vascular risk and focal neuroanatomical change, using non-invasive imaging and clinically accessible tools. It sets the stage for early, targeted CSVD risk identification and intervention, especially in individuals who are cognitively intact but at risk.

4.4. Limitations and future directions

While this study offers important insights into early white matter microstructural alterations in asymptomatic individuals with cardiocerebrovascular risk, several limitations should be acknowledged to contextualize the findings and guide future research. Firstly, our study sample had a relatively young mean age (mean 39.8 years), which may limit generalizability to older populations where CSVD is more prevalent. However, this younger cohort was intentionally selected to investigate preclinical, early-stage microstructural changes before the accumulation of a substantial WMHs burden and overt cognitive

Table 4
Correlation and multiple linear regression profile of study variables with white matter integrity.

Variables and tracts	*r (β)*			
	FA	MD	AD	RD
Age				
RACR	−0.43* (1.23)	−0.13 (−0.78)	−0.23* (−2.52)	0.00 (1.46)
LACR	−0.42* (1.15)	−0.14 (−1.96)	−0.23* (−2.44)	−0.01 (2.74)
RSCR	−0.38* (0.17)	−0.11 (−0.53)	−0.20* (0.43)	0.03 (0.16)
LSCR	−0.40* (−0.80)	−0.13 (−0.26)	−0.21* (0.74)	−0.02 (−1.26)
RSLF	−0.46* (−0.32)	−0.14 (−0.85)	−0.23* (−0.72)	−0.02 (0.27)
LSLF	−0.37* (2.76)	−0.16 (1.18)	−0.24* (−5.73)	−0.07 (4.81)
QRISK3				
RACR	−0.28* (3.90)	0.05 (−0.67)	−0.04 (−7.32)	0.16 (4.84)
LACR	−0.26* (−1.87)	0.05 (−1.41)	−0.03 (4.26)	0.15 (−2.42)
RSCR	−0.24* (0.47)	0.05 (1.44)	−0.03 (−1.86)	0.16 (0.63)
LSCR	−0.30* (−0.41)	0.05 (1.81)	−0.03 (0.69)	0.14 (−0.97)
RSLF	−0.35* (−2.94)	0.07 (−0.75)	−0.02 (5.14)	0.18 (−3.47)
LSLF	−0.35* (4.09 *)	0.06 (3.07*)	−0.03 (−9.09*)	0.17 (8.11*)
PRI				
RACR	0.45* (−3.55)	0.15 (−0.21)	0.24* (8.21)	0.03 (−4.79)
LACR	0.45* (1.69)	0.14 (0.67)	0.23* (−3.15)	0.03 (1.75)
RSCR	0.33* (2.61)	0.14 (−0.07)	0.21* (−7.64)	0.05 (4.25)
LSCR	0.39* (−1.03)	0.16 (0.76)	0.23* (5.11)	0.07 (−2.65)
RSLF	0.45* (−0.06)	0.12 (0.41)	0.21* (0.49)	0.02 (−1.47)
LSLF	0.42* (0.57)	0.16 (1.27)	0.24* (−1.67)	0.07 (1.49)
WMI				
RACR	0.28* (−0.80)	0.03 (0.08)	0.09 (1.20)	−0.06 (0.30)
LACR	0.32* (−0.14)	0.01 (0.21)	0.08 (2.30)	−0.09 (−2.20)
RSCR	0.14 (−1.17)	0.00 (−0.92)	0.05 (0.44)	−0.06 (−0.17)
LSCR	0.25* (1.95)	0.00 (0.14)	0.06 (−4.05)	−0.07 (3.13)
RSLF	0.36* (−1.85)	−0.00 (−0.07)	0.08 (5.10)	−0.11 (−4.89)
LSLF	0.28* (0.23)	0.00 (0.98)	0.07 (−0.27)	−0.06 (0.59)
PSI				
RACR	0.28* (0.49)	−0.04 (−0.79)	0.04 (−0.79)	−0.14 (1.47)
LACR	0.27* (−1.68)	−0.05 (0.82)	0.03 (3.85)	−0.15 (−3.95)
RSCR	0.20* (−0.73)	−0.06 (0.51)	0.01 (0.35)	−0.15 (0.24)
LSCR	0.31* (2.10)	−0.06 (0.90)	0.02 (−4.71)	−0.16 (3.25)
RSLF	0.35* (−0.14)	−0.07 (0.54)	0.02 (0.81)	−0.18 (−1.22)
LSLF	0.33* (−2.02)	−0.03 (0.99)	0.05 (6.11)	−0.13 (−4.10)

Notes: r = Pearson correlation coefficient; β = standardized beta coefficients; *p = significant difference (2-tailed) at the 0.01; AD, axial diffusivity; CD, cluster differentiation; FA, fractional anisotropy; LACR, left anterior corona radiata; LSCR, left superior corona radiata; LSLF, left superior longitudinal fasciculus; MD, mean diffusivity; PRI, perceptual reasoning index; PSI, processing speed

index; RACR, right anterior corona radiata; RD, radial diffusivity; RSCR, right superior corona radiata; RSLF, right superior longitudinal fasciculus; WMI, working memory index.

impairment. Future studies should include broader age ranges to validate these findings in older adults with higher vascular risk profiles. Secondly, the relatively small sample size, particularly within tract-specific subgroups (e.g., 3–7 subjects per ROI), limits the statistical power to detect subtle associations, especially in DTI metrics [70,71]. This also restricts the generalizability of our findings to broader populations. Future studies with larger, more diverse cohorts are essential to validate the observed relationships and improve confidence in the tract-specific inferences.

Third, the cross-sectional design precludes causal inference. Although we observed correlations between age, QRISK3 scores, and white matter integrity, we cannot determine whether these changes preceded, coincided with, or followed the development of WMHs and cognitive changes. Longitudinal follow-up is necessary to examine the temporal progression of microstructural damage, WMHs accumulation, and cognitive decline, and to determine whether early DTI alterations predict long-term outcomes such as vascular cognitive impairment or dementia.

Fourth, while DTI provides sensitive and non-invasive insights into white matter structure, it has known limitations. The tensor model assumes a single fiber direction per voxel, which may oversimplify complex fiber architectures, particularly in crossing fiber regions like the corona radiata and SLF [72]. More advanced diffusion models such as neurite orientation dispersion and density imaging (NODDI) [73], diffusion kurtosis imaging (DKI) [74], or free-water imaging could offer deeper pathophysiological insights by distinguishing between demyelination, axonal loss, and extracellular water content. Additionally, integrating perfusion imaging (e.g., arterial spin labelling, ASL) [75], cerebral small vessel reactivity (e.g., BOLD-based CVR mapping) [76], or magnetization transfer ratio (MTR) imaging [77,78] may provide a more comprehensive understanding of CSVD.

Fifth, although we used QRISK3 as a vascular risk stratification tool, it does not capture all CSVD-relevant variables, such as inflammatory markers, homocysteine levels, blood-brain barrier integrity, or genetic predisposition (e.g., APOE ε4 and NOTCH3). Future studies should explore multimodal risk profiling, integrating systemic, neuroimaging, and fluid biomarkers to enhance predictive precision.

Finally, although we observed trends linking FA to cognitive performance, the absence of significant group-level cognitive impairment may reflect the early-stage nature of CSVD in this cohort or ceiling effects in the cognitive assessments. Future research may benefit from using more sensitive neuropsychological batteries, computerized processing speed tests, or functional MRI to detect subtle deficits.

Despite these limitations, this study lays important groundwork by demonstrating that subtle, anatomically specific white matter changes can be detected in cognitively intact, at-risk individuals using widely available tools. This supports a preventive paradigm in CSVD research shifting from identifying irreversible damage to detecting and modifying early risk states. Future directions should include firstly longitudinal multi-timepoint DTI studies to map the trajectory of tract-specific microstructural decline. Second, multicenter population studies to enhance external validity. Third, interventional trials to assess whether lifestyle or pharmacological modifications (e.g., antihypertensives, statins, exercise) can mitigate white matter decline in high-risk but asymptomatic individuals. Finally, machine learning approaches to integrate neuroimaging, cognitive, and vascular risk data for personalized CSVD prediction models.

5. Conclusion

This study highlights the presence of early white matter microstructural alterations in anatomically specific tracts among asymptomatic individuals with elevated vascular risk, particularly as measured by QRISK3. Although conventional MRI-detected WMHs were not significantly associated with cognitive impairment, DTI revealed subtle disruptions most notably within the LSLF that correlated with increased age, vascular risk, and lower processing speed performance. By integrating lesion-guided tractography, vascular risk profiling, and cognitive testing, this study underscores the value of DTI as a sensitive tool for detecting preclinical changes in CSVD. These findings advocate for a shift toward early detection and prevention, particularly in middle-aged adults with modifiable cardiocerebrovascular risk factors. Future longitudinal and interventional research is warranted to validate these tract-specific markers and establish their predictive utility in mitigating long-term cognitive decline. Such approaches will be critical for developing precision strategies to identify, monitor, and treat individuals at risk for CSVD before it becomes irreversible.

CRediT authorship contribution statement

Zaw Myo Hein: Writing – review & editing, Writing – original draft, Visualization, Resources, Investigation, Funding acquisition, Data curation. **Muhammad Danial Che Ramli:** Writing – review & editing, Writing – original draft, Data curation. **Usman Jaffer:** Writing – review & editing, Writing – original draft, Visualization, Investigation, Data curation. **Che Mohd Nasril Che Mohd Nassir:** Writing – review & editing, Writing – original draft, Visualization, Resources, Project administration, Investigation, Data curation, Conceptualization.

Ethical statement

The study was conducted according to the guidelines of the Declaration of Helsinki and approved by the Human Research Ethics Committee at Universiti Sains Malaysia (Protocol code: USM/JEPeM/15030096). Informed consent was obtained from all subjects involved in the study.

Funding statement

This work was supported by the Fundamental Research Grant Scheme (FRGS), Ministry of Higher Education (Grant number 203/PPSP/61771193).

Declaration of competing interest

The authors declare that they have no known competing financial interests or personal relationships that could have appeared to influence the work reported in this paper.

Acknowledgements

The authors express their gratitude to Ajman University, UAE, for their support for the article processing charge (APC). We thank the management of the Hospital Pakar Universiti Sains Malaysia for granting permission to the investigators to use patient medical records as well as space and assets belonging to the hospital during the conduct of the research. The authors would also like to acknowledge that the assistance of ChatGPT 4.0, an AI language model developed by OpenAI, was used to help in the refinement of certain and limited sections of this manuscript, particularly for the language editing. Further, all AI-assisted content has been duly reviewed and thoroughly edited by the authors to ensure accuracy, scientific rigor, and adherence to the standards of academic writing. Authors are fully responsible for the content of this manuscript, even those parts improved by an AI tool, and are thus liable for any breach of publication ethics. This work was supported by the Fundamental Research Grant Scheme (FRGS), Ministry of Higher Education (Grant number 203/PPSP/61771193).

Appendix A. Supplementary data

Supplementary data to this article can be found online at https://doi.org/10.1016/j.tria.2025.100425.

References

[1] L. Pantoni, Cerebral small vessel disease: from pathogenesis and clinical characteristics to therapeutic challenges, Lancet Neurol. 9 (2010) 689–701, https://doi.org/10.1016/S1474-4422(10)70104-6.

[2] A.G. Lammie, Small vessel disease, in: H. Kalimo (Ed.), Cerebrovascular Diseases, ISN Neuropath Press, Basel, Switzerland, 2005, pp. 85–91.

[3] J. Ogata, H. Yamanishi, H. Ishibashi-Ueda, Pathology of cerebral small vessel disease, in: L. Pantoni, P.B. Gorelick (Eds.), Cerebral Small Vessel Disease, Cambridge University Press, Cambridge, UK, 2014, pp. 4–15.

[4] C.S. Thompson, A.M. Hakim, Living beyond our physiological means: small vessel disease of the brain is an expression of a systemic failure in arteriolar function: a unifying hypothesis, Stroke 40 (2009) e322–e330, https://doi.org/10.1161/STROKEAHA.108.542266.

[5] V. Hachinski, World stroke day 2008: "little strokes, big trouble", Stroke 39 (2008) 2407–2420, https://doi.org/10.1161/STROKEAHA.108.531681.

[6] A.S. Das, R.W. Regenhardt, M.W. Vernooij, D. Blacker, A. Charidimou, A. Viswanathan, Asymptomatic cerebral small vessel disease: insights from population-based studies, J. Stroke 21 (2019) 121–138, https://doi.org/10.5853/jos.2018.03608.

[7] B. Gunda, D. Bereczki, G. Várallyay, Multimodal MRI of cerebral small vessel disease, in: P. Bright (Ed.), Neuroimaging – Clinical Applications, INTECH Open Access Publisher, London, UK, 2012, pp. 277–291.

[8] M. Duering, G.J. Biessels, A. Brodtmann, et al., Neuroimaging standards for research into small vessel disease – advances since 2013, Lancet Neurol. 22 (2023) 602–618, https://doi.org/10.1016/S1474-4422(23)00131-X.

[9] E.E. Smith, G. Saposnik, G.J. Biessels, et al., Prevention of stroke in patients with silent cerebrovascular disease: a scientific statement from the American heart association/american stroke association, Stroke 48 (2017) e44–e71, https://doi.org/10.1161/STR.0000000000000116.

[10] O. Mirmosayyeb, M. Yazdan Panah, S. Vaheb, et al., Association between diffusion tensor imaging measurements and cognitive performances in people with multiple sclerosis: a systematic review and meta-analysis, Mult. Scler. Relat. Disord 94 (2025) 106261, https://doi.org/10.1016/j.msard.2025.106261.

[11] M. Bergamino, R.R. Walsh, A.M. Stokes, Free-water diffusion tensor imaging improves the accuracy and sensitivity of white matter analysis in Alzheimer's disease, Sci. Rep. 11 (2021) 6990, https://doi.org/10.1038/s41598-021-86505-7.

[12] C.D. Mayo, M.A. Garcia-Barrera, E.L. Mazerolle, et al., Relationship between DTI metrics and cognitive function in alzheimer's disease, Front. Aging Neurosci. 10 (2019) 436, https://doi.org/10.3389/fnagi.2018.00436.

[13] R. Jia, G. Solé-Guardia, A.J. Kiliaan, Blood-brain barrier pathology in cerebral small vessel disease, Neural Regen Res. 19 (2024) 1233–1240, https://doi.org/10.4103/1673-5374.385864.

[14] V. Rajeev, D.Y. Fann, Q.N. Dinh, et al., Pathophysiology of blood brain barrier dysfunction during chronic cerebral hypoperfusion in vascular cognitive impairment, Theranostics 12 (2022) 1639–1658, https://doi.org/10.7150/thno.68304.

[15] M. Mustapha, C.M.N.C. Nassir, N. Aminuddin, et al., Cerebral small vessel disease (CSVD) – lessons from the animal models, Front. Physiol. 10 (2019) 1317, https://doi.org/10.3389/fphys.2019.01317.

[16] Q. Li, Y. Yang, C. Reis, et al., Cerebral small vessel disease, Cell Transplant. 27 (2018) 1711–1722, https://doi.org/10.1177/0963689718795148.

[17] J. Hippisley-Cox, C.A.C. Coupland, M. Bafadhel, et al., Development and validation of a new algorithm for improved cardiovascular risk prediction, Nat. Med. 30 (2024) 1440–1447, https://doi.org/10.1038/s41591-024-02905-y.

[18] X. Mu, A. Wu, H. Hu, H. Zhou, M. Yang, Assessment of QRISK3 as a predictor of cardiovascular disease events in type 2 diabetes mellitus, Front. Endocrinol. 13 (2022) 1077632, https://doi.org/10.3389/fendo.2022.1077632.

[19] G.S. Collins, D.G. Altman, Predicting the 10 year risk of cardiovascular disease in the United Kingdom: independent and external validation of an updated version of QRISK2, Br. Med. J. 344 (2012) e4181, https://doi.org/10.1136/bmj.e4181.

[20] D.A. Hoagey, L.T.T. Lazarus, K.M. Rodrigue, K.M. Kennedy, The effect of vascular health factors on white matter microstructure mediates age-related differences in executive function performance, Cortex 141 (2021) 403–420, https://doi.org/10.1016/j.cortex.2021.04.016.

[21] D. Szucs, J.P. Ioannidis, Sample size evolution in neuroimaging research: an evaluation of highly-cited studies (1990–2012) and of latest practices (2017–2018) in high-impact journals, Neuroimage 221 (2020) 117164, https://doi.org/10.1016/j.neuroimage.2020.117164.

[22] T. Taoka, Y. Masutani, H. Kawai, et al., Evaluation of glymphatic system activity with the diffusion MR technique: diffusion tensor image analysis along the perivascular space (DTI-Alps) in Alzheimer's disease cases, Jpn. J. Radiol. 35 (2017) 172–178, https://doi.org/10.1007/s11604-017-0617-z.

[23] S. Kanjilal, V.S. Rao, M. Mukherjee, et al., Application of cardiovascular disease risk prediction models and the relevance of novel biomarkers to risk stratification in Asian Indians, Vasc. Health Risk Manag. 4 (2008) 199–211, https://doi.org/10.2147/vhrm.2008.04.01.199.

[24] B.V. Zlokovic, R.F. Gottesman, K.E. Bernstein, et al., Vascular contributions to cognitive impairment and dementia (VCID): a report from the 2018 NHLBI and NINDS workshop, Alzheimer's Dement. 16 (2020) 1714–1733, https://doi.org/10.1002/alz.12157.

[25] D. Wechsler, Wechsler Adult Intelligence Scale–Fourth Edition (WAIS-IV), APA PsycTests, 2008, https://doi.org/10.1037/t15169-000.

[26] L. Griffanti, M. Jenkinson, S. Suri, et al., Classification and characterization of periventricular and deep white matter hyperintensities on MRI: a study in older adults, Neuroimage 170 (2018) 174–181, https://doi.org/10.1016/j.neuroimage.2017.03.024.

[27] F. Fazekas, J.B. Chawluk, A. Alavi, H.I. Hurtig, R.A. Zimmerman, MR signal abnormalities at 1.5 T in Alzheimer's dementia and normal aging, AJR Am. J. Roentgenol. 149 (1987) 351–356, https://doi.org/10.2214/ajr.149.2.351.

[28] N. Toussaint, J.C. Souplet, P. Fillard, MedINRIA: medical image navigation and research tool by INRIA, in: Proc of MICCAI'07 Workshop on Interaction in Medical Image Analysis and Visualization, Brisbane, Australia, 2007. https://inria.hal.science/inria-00616047v1.

[29] F.F. Zhai, Li ML. YanS, F. Han, Q. Wang, L.X. Zhou, J. Ni, M. Yao, S.Y. Zhang, L. Y. Cui, Z.Y. Jin, Y.C. Zhu, Intracranial arterial dolichoectasia and stenosis: risk factors and relation to cerebral small vessel disease, Stroke 49 (2018) 1135–1140, https://doi.org/10.1161/STROKEAHA.117.020130.

[30] F.C. Yeh, T.D. Verstynen, Y. Wang, et al., Deterministic diffusion fiber tracking improved by quantitative anisotropy, PLoS One 8 (2013) e80713, https://doi.org/10.1371/journal.pone.0080713.

[31] W.M.A.W. Ahmad, N.U.M. Allah, M.S.M. Ibrahim, et al., Using decision tree and response surface methodology to review chronic periodontitis profile in Pakistan: a preliminary case study, Int. J. Eng. Technol. 7 (2018) 76–79, https://doi.org/10.14419/ijet.v7i3.28.20971.

[32] C.W. van der Weijden, A. van der Hoorn, J.H. Potze, et al., Diffusion-derived parameters in lesions, peri-lesion and normal-appearing white matter in multiple sclerosis using tensor, kurtosis and fixel-based analysis, J. Cerebr. Blood Flow Metabol. 42 (2022) 2095–2106, https://doi.org/10.1177/0271678X221107953.

[33] W.Y. Aung, S. Mar, T.L. Benzinger, Diffusion tensor MRI as a biomarker in axonal and myelin damage, Imag. Med. 5 (2013) 427–440, https://doi.org/10.2217/iim.13.49.

[34] M. Duering, S. Finsterwalder, E. Baykara, et al., Free water determines diffusion alterations and clinical status in cerebral small vessel disease, Alzheimer's Dement. 14 (2018) 764–774, https://doi.org/10.1016/j.jalz.2017.12.007.

[35] A. Heckel, M. Weiler, A. Xia, et al., Peripheral nerve diffusion tensor imaging: assessment of axon and myelin sheath integrity, PLoS One 10 (2015) e0130833, https://doi.org/10.1371/journal.pone.0130833.

[36] I.J. Bennett, D.J. Madden, C.J. Vaidya, et al., Age-related differences in multiple measures of white matter integrity: a diffusion tensor imaging study of healthy aging, Hum. Brain Mapp. 31 (2010) 378–390, https://doi.org/10.1002/hbm.20872.

[37] S. Keihaninejad, N.S. Ryan, I.B. Malone, et al., The importance of group-wise registration in tract based spatial statistics study of neurodegeneration: a simulation study in alzheimer's disease, PLoS One 7 (2012) e45996, https://doi.org/10.1371/journal.pone.0045996.

[38] M.R. Nelson, E.G. Keeling, A.M. Stokes, M. Bergamino, Exploring white matter microstructural alterations in mild cognitive impairment: a multimodal diffusion MRI investigation utilizing diffusion kurtosis and free-water imaging, Front. Neurosci. 18 (2024) 1440653, https://doi.org/10.3389/fnins.2024.1440653.

[39] Y. Wang, G. Liu, D. Hong, et al., White matter injury in ischemic stroke, Prog. Neurobiol. 141 (2016) 45–60, https://doi.org/10.1016/j.pneurobio.2016.04.005.

[40] O.R. Phillips, S.H. Joshi, F. Piras, et al., The superficial white matter in alzheimer's disease, Hum. Brain Mapp. 37 (2016) 1321–1334, https://doi.org/10.1002/hbm.23105.

[41] T. Burke, L. Holleran, D. Mothersill, et al., Bilateral anterior Corona radiata microstructure organisation relates to impaired social cognition in schizophrenia, Schizophr. Res. 262 (2023) 87–94, https://doi.org/10.1016/j.schres.2023.10.035.

[42] L. Lin, Y. Xue, Q. Duan, et al., Microstructural white matter abnormalities and cognitive dysfunction in subcortical ischemic vascular disease: an atlas-based diffusion tensor analysis study, J. Mol. Neurosci. 56 (2015) 363–370, https://doi.org/10.1007/s12031-015-0550-5.

[43] X. Wang, S. Pathak, L. Stefaneanu, et al., Subcomponents and connectivity of the superior longitudinal fasciculus in the human brain, Brain Struct. Funct. 221 (2016) 2075–2092, https://doi.org/10.1007/s00429-015-1028-5.

[44] R.P. Cabeen, M.E. Bastin, D.H. Laidlaw, A comparative evaluation of voxel-based spatial mapping in diffusion tensor imaging, Neuroimage 146 (2017) 100–112, https://doi.org/10.1016/j.neuroimage.2016.11.020.

[45] S.N. Kashefi, G.P. Winston, Diffusion tensor imaging, in: M. Mannil, S. X. Winklhofer (Eds.), Neuroimaging Techniques in Clinical Practice, Springer, Cham, 2020, https://doi.org/10.1007/978-3-030-48419-4_14.

[46] A.C. Seifert, M. Umphlett, M. Hefti, M. Fowkes, J. Xu, Formalin tissue fixation biases myelin-sensitive MRI, Magn. Reson. Med. 82 (2019) 1504–1517, https://doi.org/10.1002/mrm.27821.

[47] E. Alonso-Ortiz, I.R. Levesque, G.B. Pike, MRI-Based myelin water imaging: a technical review, Magn. Reson. Med. 73 (2015) 70–81, https://doi.org/10.1002/mrm.25198.

[48] P. Ravanfar, S.M. Loi, W.T. Syeda, et al., Systematic review: quantitative susceptibility mapping (QSM) of brain iron profile in neurodegenerative diseases, Front. Neurosci. 15 (2021) 618435, https://doi.org/10.3389/fnins.2021.618435.

[49] P. van Gelderen, J.A. de Zwart, J.H. Duyn, Pitfalls of MRI measurement of white matter perfusion based on arterial spin labeling, Magn. Reson. Med. 59 (2008) 788–795, https://doi.org/10.1002/mrm.21515.

[50] P. Lenga, M. Scherer, P. Neher, et al., Tensor- and high-resolution fiber tractography for the delineation of the optic radiation and corticospinal tract in the

proximity of intracerebral lesions: a reproducibility and repeatability study, Acta Neurochir. 165 (2023) 1041–1051, https://doi.org/10.1007/s00701-023-05540-7.
[51] J.Y. Yang, C.H. Yeh, C. Poupon, F. Calamante, Diffusion MRI tractography for neurosurgery: the basics, current state, technical reliability and challenges, Phys. Med. Biol. 66 (2021) 15, https://doi.org/10.1088/1361-6560/ac0d90.
[52] S.J. van Veluw, K. Arfanakis, J.A. Schneider, Neuropathology of vascular brain health: insights from ex vivo magnetic resonance imaging-histopathology studies in cerebral small vessel disease, Stroke 53 (2022) 404–415, https://doi.org/10.1161/STROKEAHA.121.032608.
[53] K.E. McAleese, I. Alafuzoff, A. Charidimou, et al., Post-mortem assessment in vascular dementia: advances and aspirations, BMC Med. 14 (2016) 129, https://doi.org/10.1186/s12916-016-0676-5.
[54] R. Moretti, P. Caruso, Small vessel disease: ancient description, novel biomarkers, Int. J. Mol. Sci. 23 (2022) 3508, https://doi.org/10.3390/ijms23073508.
[55] J.M. Wardlaw, C. Smith, M. Dichgans, Small vessel disease: mechanisms and clinical implications, Lancet Neurol. 18 (2019) 684–696, https://doi.org/10.1016/S1474-4422(19)30079-1.
[56] Y. Shi, J.M. Wardlaw, Update on cerebral small vessel disease: a dynamic whole-brain disease, Stroke Vasc. Neurol. 1 (2016) 83–92, https://doi.org/10.1136/svn-2016-000035.
[57] X. Yu, X. Yin, H. Hong, et al., Increased extracellular fluid is associated with white matter fiber degeneration in CADASIL: in vivo evidence from diffusion magnetic resonance imaging, Fluids Barriers CNS 18 (2021) 29, https://doi.org/10.1186/s12987-021-00264-1.
[58] A. Seehaus, A. Roebroeck, M. Bastiani, et al., Histological validation of high-resolution DTI in human postmortem tissue, Front. Neuroanat. 9 (2015) 98, https://doi.org/10.3389/fnana.2015.00098.
[59] M. Seki, H. Yoshizawa, M. Hosoya, K. Kitagawa, Neuropsychological profile of early cognitive impairment in cerebral small vessel disease, Cerebrovasc. Dis. 51 (2022) 600–607, https://doi.org/10.1159/000522438.
[60] O. Hamilton, S.R. Cox, L. Ballerini, et al., Associations between total MRI-Visible small vessel disease burden and domain-specific cognitive abilities in a community-dwelling older-age cohort, Neurobiol. Aging 105 (2021) 25–34, https://doi.org/10.1016/j.neurobiolaging.2021.04.007.
[61] H.M. Genova, J. DeLuca, N. Chiaravalloti, G. Wylie, The relationship between executive functioning, processing speed, and white matter integrity in multiple sclerosis, J. Clin. Exp. Neuropsychol. 35 (2013) 631–641, https://doi.org/10.1080/13803395.2013.806649.
[62] G.A. Kerchner, C.A. Racine, S. Hale, et al., Cognitive processing speed in older adults: relationship with white matter integrity, PLoS One 7 (2012) e50425, https://doi.org/10.1371/journal.pone.0050425.
[63] K.L. Moran, C.J. Smith, E. McManus, et al., Cerebrovascular health impacts processing speed through anterior white matter alterations: a UK biobank study, Sci. Rep. 15 (2025) 9860, https://doi.org/10.1038/s41598-025-93399-2.
[64] A. Mendez Colmenares, M.L. Thomas, C. Anderson, et al., Testing the structural disconnection hypothesis: myelin content correlates with memory in healthy aging, Neurobiol. Aging 141 (2024) 21–33, https://doi.org/10.1016/j.neurobiolaging.2024.05.013.
[65] Q. Fu, Y. Qiu, Y. Hu, et al., Free water-corrected fractional anisotropy in normal-appearing white matter as a potential neuroimaging biomarker for attention and executive function impairment in cerebral small vessel disease, CNS Neurosci. Ther. 31 (2025) e70475, https://doi.org/10.1111/cns.70475.
[66] A.T. Siddiquee, Y.H. Hwang, S. Kim, et al., Middle-age cerebral small vessel disease and cognitive function in later life: a population-based prospective cohort study, Lancet Reg. Health West Pac. 55 (2025) 101284, https://doi.org/10.1016/j.lanwpc.2024.101284.
[67] F.M. Elahi, M.M. Wang, J.F. Meschia, Cerebral small vessel disease-related dementia: more questions than answers, Stroke 54 (2023) 648–660, https://doi.org/10.1161/STROKEAHA.122.038265.
[68] L. Chouliaras, J.T. O'Brien, The use of neuroimaging techniques in the early and differential diagnosis of dementia, Mol. Psychiatr. 28 (2023) 4084–4097, https://doi.org/10.1038/s41380-023-02215-8.
[69] L. Lang, Y. Wang, Markov model combined with MR diffusion tensor imaging for predicting the onset of alzheimer's disease, Open Life Sci. 18 (2023) 20220714, https://doi.org/10.1515/biol-2022-0714.
[70] C.M. Bögerl, F.B. Laun, A.M. Nagel, et al., Analysis of the sample size used in clinical MRI studies, PLoS One 20 (2025) e0316611, https://doi.org/10.1371/journal.pone.0316611.
[71] M. Egle, S. Hilal, A.M. Tuladhar, et al., Determining the optimal DTI analysis method for application in cerebral small vessel disease, Neuroimage Clin. 35 (2022) 103114, https://doi.org/10.1016/j.nicl.2022.103114.
[72] Z. Jin, Y. Bao, Y. Wang, et al., Differences between generalized Q-sampling imaging and diffusion tensor imaging in visualization of crossing neural fibers in the brain, Surg. Radiol. Anat. 41 (2019) 1019–1028, https://doi.org/10.1007/s00276-019-02264-1.
[73] F. Spagnolo, S. Gobbi, E. Zsoldos, et al., Down-sampling in diffusion MRI: a bundle-specific DTI and NODDI study, Front Neuroimag. 3 (2024) 1359589, https://doi.org/10.3389/fnimg.2024.1359589.
[74] A. Arab, A. Wojna-Pelczar, A. Khairnar, et al., Principles of diffusion kurtosis imaging and its role in early diagnosis of neurodegenerative disorders, Brain Res. Bull. 139 (2018) 91–98, https://doi.org/10.1016/j.brainresbull.2018.01.015.
[75] X. Wang, Y. Wang, D. Gao, et al., Characterizing the penumbras of white matter hyperintensities in patients with cerebral small vessel disease, Jpn. J. Radiol. 41 (2023) 928–937, https://doi.org/10.1007/s11604-023-01419-w.
[76] X. Hou, P. Liu, Y. Li, et al., The association between BOLD-Based cerebrovascular reactivity (CVR) and end-tidal CO2 in healthy subjects, Neuroimage 207 (2020) 116365, https://doi.org/10.1016/j.neuroimage.2019.116365.
[77] F.B.C. Macruz, F.S. Feltrin, A. Zaninotto, et al., Longitudinal assessment of magnetization transfer ratio, brain volume, and cognitive functions in diffuse axonal injury, Brain Behav. 12 (2022) e2490, https://doi.org/10.1002/brb3.2490.
[78] C.H. Lee, P. Walczak, J. Zhang, Inhomogeneous magnetization transfer MRI of white matter structures in the hypomyelinated shiverer mouse brain, Magn. Reson. Med. 88 (2022) 332–340, https://doi.org/10.1002/mrm.29207.